Commun. Comput. Phys.
doi: 10.4208/cicp.250110.160211a

Vol. **11**, No. 3, pp. 1022-1042
March 2012

Modified Upwinding Compact Scheme for Shock and Shock Boundary Layer Interaction

Chaoqun Liu*, Ping Lu, Maria Oliveira and Peng Xie

Department of Mathematics, University of Texas at Arlington, Arlington, TX 76019, USA.

Received 25 January 2010; Accepted (in revised version) 16 February 2011

Communicated by Kun Xu

Available online 18 November 2011

Abstract. Standard compact scheme and upwinding compact scheme have high order accuracy and high resolution, but cannot capture the shock which is a discontinuity. This work developed a modified upwinding compact scheme which uses an effective shock detector to block compact scheme to cross the shock and a control function to mix the flux with WENO scheme near the shock. The new scheme makes the original compact scheme able to capture the shock sharply and, more importantly, keep high order accuracy and high resolution in the smooth area which is particularly important for shock boundary layer and shock acoustic interactions. Numerical results show the scheme is successful for 2-D Euler and 2-D Navier-Stokes solvers. The examples include 2-D incident shock, 2-D incident shock and boundary layer interaction. The scheme is robust, which does not involve case related parameters.

PACS: 47.11.-j, 47.11.Bc

Key words: Compact scheme, WENO, shock-boundary layer interaction, shock detector.

Nomenclature

M_∞	Mach number	Re	Reynolds number
P	Pressure	ρ	Density
U	Velocity	E	Internal energy
f	Original function	$\hat{f}$	Flux at the cell interface
F	Original function	H	Primitive function of $\hat{f}$
IS	WENO smoothness	ω	WENO weights
Ω	Control function		
T_C	Truncation error on coarse grid	T_F	Truncation error on fine grid
MR	Multigrid truncation error ratio	LR	Local left and right slope ratio
CS	Compact Scheme	MUCS	Modified upwinding compact scheme

*Corresponding author. *Email addresses:* cliu@uta.edu (C. Liu), ping.lu@mavs.uta.edu (P. Lu), malubamol@gmail.com (M. Oliveira), xiepeng.peng@gmail.com (P. Xie)

 ©2012 Global-Science Press

1 Introduction

The flow field is in general governed by the Navier-Stokes system which is a system of time dependent partial differential equations. However, for external flows, the viscosity is important largely only in the boundary layers. The main flow can still be considered as inviscid and the governing system can be dominated by the time dependent Euler equations which are hyperbolic. The difficult problem with numerical solution is the shock capturing which can be considered as a discontinuity or mathematical singularity (no classical unique solution and no bounded derivatives). In the shock area, continuity and differentiability of the governing Euler equations are lost and only the weak solution in an integration form can be obtained. The shock can be developed in some cases because the Euler equation is non-linear and hyperbolic. On the other hand, the governing Navier-Stokes system presents parabolic type behavior and is therefore dominated by viscosity or second order derivatives in the boundary layer. One expects that the equation should be solved by a high order compact scheme to get high order accuracy and high resolution. High order of accuracy is critical in resolving small length scales in flow transition and turbulence processes. However, for hyperbolic systems, the analysis already shows the existence of characteristic lines and Riemann invariants. Apparently, the upwind finite difference scheme coincides with the physics for a hyperbolic system. History has shown the great success of upwind technologies. From the point of view of shocks, it makes no sense to use high order compact schemes for shock capturing. High order compact schemes use all gird points on one grid line to calculate the derivative by solving a tri-diagonal or penta-diagonal linear system. However, the shock does not have finite derivatives and downstream quantities cannot cross shock to affect the upstream points. From the point of view of the above statements, upwind scheme is appropriate for the hyperbolic system. Many upwind or bias upwind schemes have achieved great success in capturing the shocks sharply, such as [4, 15], MUSCL [21], TVD [5], ENO [6, 17, 18] and WENO (see [7, 12]). All these shock-capturing schemes are based on upwind or bias upwind technology, which is nice for hyperbolic systems, but is not favorable to the N-S system which presents parabolic equation behavior. The small length scale is very important in the flow transition and turbulence process and thus very sensitive to any artificial numerical dissipation. High order compact schemes (see [10, 22]) are more appropriate for simulation of flow transition and turbulence because it is central and non-dissipative with high order accuracy and high resolution.

Unfortunately, the shock-boundary layer interaction, which is important to high speed flow, is a mixed type problem which has shock (discontinuity), boundary layer (viscosity), separation, transition, expansion fans, fully developed turbulence, and reattachment. In the case of shock-boundary layer interaction, there are elliptic (parabolic for time dependent problems) areas (separation, transition, turbulence) and hyperbolic areas (main flow, shocks, expansion fans), which makes the accurate numerical simulation extremely difficult if not impossible. We may divide the computational domain into several parts: the elliptic (parabolic for time dependent problems), hyperbolic, and mixed.

The division or detection can be performed by a switch function automatically such as shock detectors which simply sets $\Omega=1$ for the shock area and $\Omega=0$ for the rest. The switch function may give good results for shock-boundary layer interaction, but it will have too many logical statements in the code which may slow down the computation. The switch function could also be case-related and very difficult to adjust. It would also slow down the convergence for steady problems.

A combination of compact and WENO schemes should be desirable. There are some efforts to combine WENO with standard central (see [1, 9]) and WENO with upwinding compact (UCS) schemes (see [1, 14]). Their mixing function is still some kind complex and has a number of case related adjustable coefficients.

In order to overcome the drawback of the CS scheme, we need to achieve local dependency in shock regions and recover the global dependency in smooth regions. This fundamental idea will naturally lead to a combination of a local dependent scheme, e.g., WENO and global dependent upwinding compact schemes.

This effort is to use WENO to improve a 7^{th} order upwinding compact scheme as we called as "modified upwinding compact scheme (MUCS)", which uses a new shock detector to find the shock location and a new control function to mix the upwinding compact scheme. The mixing function is designed in the following ways: the new scheme automatically becomes bias when approaching the shock, but rapidly recovers to be upwinding compact, with high order of accuracy and high resolution.

A few black box type subroutines are written and users can use a compact scheme for shock and shock boundary layer interaction by calling these subroutines.

2 Compact and WENO schemes

2.1 Compact scheme

Before discussing our new scheme, first let us see how to construct the CS and WENO schemes.

2.1.1 Primitive function for conservation

For 1-D conservation laws:

$$u_t(x,t)+f_x(u(x,t))=0. \tag{2.1}$$

When a conservative approximation to the spatial derivative is applied, a semi-discrete conservative form of the Eq. (2.1) is described as follows:

$$\frac{du_j}{dt}=-\frac{1}{\Delta x}\left(\hat{f}_{j+\frac{1}{2}}-\hat{f}_{j-\frac{1}{2}}\right), \tag{2.2}$$

where

$$f_j=\frac{1}{\Delta x}\int_{x_j-\frac{\Delta x}{2}}^{x_j+\frac{\Delta x}{2}}\hat{f}(\xi)d\xi,$$

and then

$$(f_x)_j = -\frac{1}{\Delta x}(\hat{f}_{j+\frac{1}{2}} - \hat{f}_{j-\frac{1}{2}}).$$

Note that f is the original function, but $\hat{f}$ is the flux defined by the above integration. Eq. (2.2) is an exact formula for the flux, but $\hat{f}$ is different from f.

Let H be the primitive function of $\hat{f}$ defined below:

$$H(x_{j+\frac{1}{2}}) = \int_{-\infty}^{x_j+\frac{\Delta x}{2}} \hat{f}(\xi)d\xi = \sum_{i=-\infty}^{i=j} \int_{x_i-\frac{\Delta x}{2}}^{x_i+\frac{\Delta x}{2}} \hat{f}(\xi)d\xi = \Delta x \sum_{i=-\infty}^{j} f_i. \tag{2.3}$$

H is easy to calculate, but it is a discrete function. The numerical flux $\hat{f}$ at the cell interfaces is the derivative of its primitive function H, i.e.,

$$\hat{f}_{j+\frac{1}{2}} = H'_{j+\frac{1}{2}}. \tag{2.4}$$

All formulae given above are exact without approximations. However, the primitive function H is a discrete function and we have to use numerical methods to get the derivatives. This will introduce numerical errors.

This procedure, $f \to H \to \hat{f} \to f'_x$, was introduced by [17, 18]. There is still one problem left for numerical methods, which is how to solve (2.4) or how to get more accurate approximation for derivatives of a discrete data set $H_{j+1/2}$.

2.1.2 Data normalization

In order to find a universal formula, we need to normalize the data set, $u(i)$, $i = 1, \cdots, n$,

$$u_{diff} = |u_{\max} - u_{\min}|, \tag{2.5a}$$

$$\overline{u} = \frac{u - u_{\min}}{u_{diff}}. \tag{2.5b}$$

Here, $u_{\max}$ and $u_{\min}$ are the maximum and minimum values of u respectively and $\overline{u}$ is normalized. For simplicity, we throw out the hat of u and use $u(i)$ as the normalized data set.

2.1.3 High-order compact schemes

Traditional finite difference schemes use the idea of Lagrange interpolation. To obtain n^{th} order of accuracy, a stencil covering $n+1$ grid points is needed. In other words, the derivative at a certain grid point depends upon the function values at these $n+1$ grid points and only these grid points. In contrast, standard compact schemes (see [10, 22]) use the idea of Hermitian interpolation. By using derivatives as well as function values, a compact scheme achieves high order of accuracy without increasing the width of stencils. As discussed in Lele's paper, a compact scheme has not only high order of accuracy, but

also high resolution. Fourier analysis indicates that, with the same order of accuracy, a compact scheme has better spectral resolution than a traditional, explicit finite difference scheme. For this reason, compact schemes are favorable in the simulation of turbulent flows where small-length-scale structures are important. Due to the usage of derivatives, compact schemes usually give us a tri-diagonal or penta-diagonal system. Although the tri-diagonal matrix is sparse, the inverse of a tri-diagonal matrix is dense, which means the derivative at a certain grid point depends upon all the grid points along a grid line. The success of compact schemes indicates that the global dependency is very important for high resolution. However, while the global dependency is good for resolution it is not so applicable for shock capturing.

A Pade-type compact scheme could be constructed based on the Hermite interpolation where both function and derivatives at grid points are involved, e.g., an eighth order finite difference scheme can be constructed if both the function and first order derivative are used at five grid points. For a function f, we may write a compact scheme by using five grid points [10]:

$$\beta_- f'_{j-2}+\alpha_- f'_{j-1}+f'_j+\alpha_+ f'_{j+1}+\beta_+ f'_{j+2}=\frac{b_- f_{j-2}+\alpha_- f_{j-1}+cf_j+\alpha_+ f_{j+1}+b_+ f_{j+2}}{h}. \quad (2.6)$$

We can get 8^{th} order accuracy by using the above formula based on Taylor series.

If we use a symmetric and tri-diagonal system, by setting $\beta_-=\beta_+=0$, we can get a one parameter family of compact schemes [10]:

$$\alpha f'_{i-1}+f'_i+\alpha f'_{i+1}=\frac{1}{h}\Big[-\frac{1}{12}(4\alpha-1)f_{i-2}-\frac{1}{3}(\alpha+2)f_{j-1}+\frac{1}{3}(\alpha+2)f_{j+1}+\frac{1}{12}(4\alpha-1)f_{i+2}\Big]. \quad (2.7)$$

If $\alpha=1/3$, we will get a standard sixth order compact scheme

$$\frac{1}{3}f'_{i-1}+f'_i+\frac{1}{3}f'_{i+1}=h^{-1}\Big[-\frac{1}{36}f_{i-2}-\frac{7}{9}f_{j-1}+\frac{7}{9}f_{j+1}+\frac{1}{36}f_{i+2}\Big]. \quad (2.8)$$

Note that we only use the compact scheme (CS) for the derivative of the primitive function to get the flux: $\hat{f}_{j+1/2}=H'_{j+1/2}$.

2.1.4 Upwinding compact scheme

The standard compact scheme does not have dissipation (non-dissipative scheme) and needs a filter even for smooth area. The upwinding compact scheme can keep the high order without the filter. Following our conservative primitive function approach, the 7^{th} order up-winding scheme can be described as follows:

For the positive primitive function H^+:

1) Interior points

$$\begin{aligned}&\frac{1}{2}H'_{j-\frac{3}{2}}+H'_{j-\frac{1}{2}}+\frac{1}{4}H'_{j+\frac{1}{2}}\\&=\frac{1}{h}\Big(\frac{1}{240}H_{j-\frac{7}{2}}-\frac{1}{12}H_{j-\frac{5}{2}}-\frac{11}{12}H_{j-\frac{3}{2}}+\frac{1}{3}H_{j-\frac{1}{2}}+\frac{31}{48}H_{j+\frac{1}{2}}+\frac{1}{60}H_{j+\frac{3}{2}}\Big).\end{aligned} \quad (2.9)$$

2) For boundary points

Point 0

$$\begin{aligned}&H'_{j-\frac{1}{2}}+6H'_{j+\frac{1}{2}}\\&=\frac{1}{h}\Big(-\frac{69}{20}H_{j-\frac{1}{2}}-\frac{17}{10}H_{j+\frac{1}{2}}+\frac{15}{2}H_{j+\frac{3}{2}}-\frac{10}{3}H_{j+\frac{5}{2}}+\frac{5}{4}H_{j+\frac{7}{2}}-\frac{3}{10}H_{j+\frac{9}{2}}+\frac{1}{30}H_{j+\frac{11}{2}}\Big).\end{aligned}\tag{2.10}$$

Point 1

$$\begin{aligned}&\frac{1}{10}H'_{j-\frac{3}{2}}+H'_{j-\frac{1}{2}}+H'_{j+\frac{1}{2}}\\&=\frac{1}{h}\Big(-\frac{227}{600}H_{j-\frac{3}{2}}-\frac{13}{12}H_{j-\frac{1}{2}}+\frac{7}{6}H_{j+\frac{1}{2}}+\frac{1}{3}H_{j+\frac{3}{2}}-\frac{1}{24}H_{j+\frac{5}{2}}+\frac{1}{300}H_{j+\frac{7}{2}}\Big).\end{aligned}\tag{2.11}$$

Point 2

$$\begin{aligned}&\frac{1}{4}H'_{j-\frac{3}{2}}+H'_{j-\frac{1}{2}}+\frac{1}{2}H'_{j+\frac{1}{2}}\\&=\frac{1}{h}\Big(-\frac{1}{60}H_{j-\frac{5}{2}}-\frac{31}{48}H_{j-\frac{3}{2}}-\frac{1}{3}H_{j-\frac{1}{2}}+\frac{11}{12}H_{j+\frac{1}{2}}+\frac{1}{12}H_{j+\frac{3}{2}}-\frac{1}{240}H_{j+\frac{5}{2}}\Big).\end{aligned}\tag{2.12}$$

Point $N-1$

$$\begin{aligned}&H'_{j-\frac{3}{2}}+H'_{j-\frac{1}{2}}+\frac{1}{10}H'_{j+\frac{1}{2}}\\&=\frac{1}{h}\Big(-\frac{1}{300}H_{j-\frac{9}{2}}+\frac{1}{24}H_{j-\frac{7}{2}}-\frac{1}{3}H_{j-\frac{5}{2}}-\frac{7}{6}H_{j-\frac{3}{2}}+\frac{13}{12}H_{j-\frac{1}{2}}+\frac{227}{600}H_{j+\frac{1}{2}}\Big).\end{aligned}\tag{2.13}$$

Point N

$$\begin{aligned}&6H'_{j-\frac{3}{2}}+H'_{j-\frac{1}{2}}\\&=\frac{1}{h}\Big(-\frac{1}{30}H_{j-\frac{13}{2}}+\frac{3}{10}H_{j-\frac{11}{2}}-\frac{5}{4}H_{j-\frac{9}{2}}+\frac{10}{3}H_{j-\frac{7}{2}}-\frac{15}{2}H_{j-\frac{5}{2}}+\frac{17}{10}H_{j-\frac{3}{2}}+\frac{69}{20}H_{j-\frac{1}{2}}\Big).\end{aligned}\tag{2.14}$$

For the negative primitive function H^-, the formula is similar. Here, H^+ represents the primitive function of the positive flux and H^- represents the primitive function of the negative flux. A Lax-Friedrich flux splitting is applied in all computational examples.

2.2 WENO scheme [7]

The basic idea proposed in ENO (see [6]) and WENO (see [7]) schemes is to avoid the stencil containing a shock. ENO chooses the smoothest stencil from several candidates to calculate the derivatives. WENO controls the contributions of different stencils according to their smoothness. In this way, the derivative at a certain grid point, especially one near the shock, is dependent on a very limited number of grid points. The local dependency here is favorable for shock capturing and helps capture the non-oscillatory property. The success of ENO and WENO schemes indicate that the local dependency is critical for shock capturing.

2.2.1 Conservation form of derivative

$$\frac{\partial U}{\partial t}+\frac{\partial F}{\partial x}=0. \tag{2.15}$$

The ENO reconstruction can provide a semi-discretization for the derivative:

$$\frac{\partial F}{\partial x}=\frac{\hat{F}_{i+\frac{1}{2}}-\hat{F}_{i-\frac{1}{2}}}{\Delta x},$$

where $\hat{F}$ is the flux which must be accurately obtained.

2.2.2 5^{th} order WENO (bias upwind)

1) Flux approximation

In order to get a high order approximation for $\hat{F}_{j-1/2}=H'_{j-1/2}$, we can use three different candidates (Fig. 1) which are all third order polynomials:

E_0: $H_{j-\frac{7}{2}}, H_{j-\frac{5}{2}}, H_{j-\frac{3}{2}}, H_{j-\frac{1}{2}}$; E_1: $H_{j-\frac{5}{2}}, H_{j-\frac{3}{2}}, H_{j-\frac{1}{2}}, H_{j+\frac{1}{2}}$; E_2: $H_{j-\frac{3}{2}}, H_{j-\frac{1}{2}}, H_{j+\frac{1}{2}}, H_{j+\frac{3}{2}}$.

Let us look at candidate E_0 first. Assume H is a third order polynomial:

$$H=a_0+a_1\left(x-x_{j-\frac{1}{2}}\right)+a_2\left(x-x_{j-\frac{1}{2}}\right)^2+a_3\left(x-x_{j-\frac{3}{2}}\right)^3,$$

we can have

$$E_0\colon \hat{F}_{j-\frac{1}{2}}=\frac{1}{3}F_{j-3}-\frac{7}{6}F_{j-2}+\frac{11}{6}F_{j-1}, \tag{2.16a}$$

$$E_1\colon \hat{F}_{j-\frac{1}{2}}=-\frac{1}{6}F_{j-2}+\frac{5}{6}F_{j-1}+\frac{1}{3}F_j, \tag{2.16b}$$

$$E_2\colon \hat{F}_{j-\frac{1}{2}}=\frac{1}{3}F_{j-1}+\frac{5}{6}F_j-\frac{1}{6}F_{j+1}. \tag{2.16c}$$

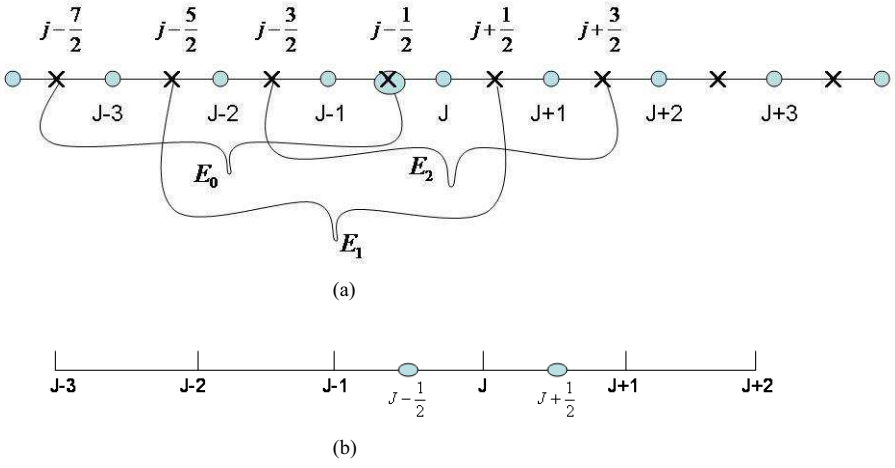

Figure 1: (a) WENO candidates. (b) 5^{th} order WENO scheme.

2) Optimal weights for high order of accuracy

The final scheme should be a combination of the three candidates:

$$E=C_0E_0+C_1E_1+C_2E_2.$$

If we set $C_0=1/10$, $C_1=6/10$, $C_2=3/10$, we will have

$$\frac{\partial F}{\partial x}=\frac{\hat{F}_{j+\frac{1}{2}}-\hat{F}_{j=\frac{1}{2}}}{\Delta x}=\frac{1}{\Delta x}\Big(-\frac{1}{30}F_{j-3}+\frac{1}{4}F_{j-2}-F_{j-1}+\frac{1}{3}F_j+\frac{1}{2}F_{j+1}-\frac{1}{20}F_{j+2}\Big)+\mathcal{O}(\Delta x^5).$$

Using the Taylor expansion for F_{j-k}, we find

$$\frac{\partial F}{\partial x}=\frac{\hat{F}_{j+\frac{1}{2}}-\hat{F}_{j-\frac{1}{2}}}{\Delta x}=F_j'-\frac{1}{60}(\Delta x)^5F_j^{(6)}+\frac{1}{140}(\Delta x)^6F_j^{(7)}+\cdots, \tag{2.17}$$

which shows that the scheme with optimal weights and 6 grid points has a 5$^{\text{th}}$ order truncation error. Note that the scheme is a **STANDARD** 5$^{\text{th}}$ order bias upwind finite difference scheme.

3) Bias upwind weights

Let us define a bias weight for each candidate according to WENO:

$$\omega_k=\gamma_k\Big(\sum_{i=0}^{2}\gamma_i\Big)^{-1},\qquad \gamma_k=\frac{C_k}{(\varepsilon+IS_k)^p}, \tag{2.18}$$

where

$$\begin{aligned}
IS_i&=\int_{x_{j-\frac{1}{2}}}^{x_{j+\frac{1}{2}}}\sum_{k=1}^{\infty}\big[p_2(x)^{(k)}\big]^2h^{2k-1}dx,\\
IS_0&=\frac{13}{12}(F_{j-2}-2F_{j-1}+F_j)^2+\frac{1}{4}(F_{j-2}-4F_{j-1}+3F_j)^2,\\
IS_1&=\frac{13}{12}(F_{j-1}-2F_j+F_{j+1})^2+\frac{1}{4}(F_{j-1}-F_{j+1})^2,\\
IS_2&=\frac{13}{12}(F_j-2F_{j+1}+F_{j+2})^2+\frac{1}{4}(F_{j+2}-4F_{j+1}+3F_j)^2.
\end{aligned}$$

The 5$^{\text{th}}$ order WENO can be obtained

$$\hat{F}_{j-\frac{1}{2}}=\omega_0E_0+\omega_1E_1+\omega_2E_2, \tag{2.19a}$$

$$\begin{aligned}
\hat{F}_{j-\frac{1}{2}}=&\omega_{0,j-\frac{1}{2}}\Big(\frac{1}{3}F_{j-3}-\frac{7}{6}F_{j-2}+\frac{11}{6}F_{j-1}\Big)+\omega_{1,j-\frac{1}{2}}\Big(-\frac{1}{6}F_{j-2}+\frac{5}{6}F_{j-1}+\frac{1}{3}F_j\Big)\\
&+\omega_{2,j-\frac{1}{2}}\Big(\frac{1}{3}F_{j-1}+\frac{5}{6}F_j-\frac{1}{6}F_{j+1}\Big).
\end{aligned} \tag{2.19b}$$

WENO is a scheme with great successes by many users. However, since the scheme has 5$^{\text{th}}$ order dissipation everywhere and third order dissipation near the shock, some researchers in the DNS/LES community still consider the scheme is too dissipative for flow transition and turbulence. Let us turn to compact schemes for assistance.

3 Modified compact scheme

Compact scheme is great to resolve small length scales, but cannot be used for the cases when a shock or discontinuity is involved. Our new modified compact scheme is an effort to remove the weakness by introducing WENO flux when the computation is approaching the shock.

3.1 Effective new shock detector

A very effective shock detector [13] has been proposed by C. Liu. The detector has two steps. The first step is to check the ratio of the truncation errors on the coarse and fine grids and the second step is to check the local ratio of the left and right hand slopes. The currently popular shock/discontinuity detectors such as Harten's, Jameson's and WENO can detect shocks, but mistake high frequency waves and critical points as shocks. The schemes then damp the physically important high frequency waves. Preliminary results show that the new shock/discontinuity detector is very delicate. The new detector can detect all shocks including strong, weak and oblique shocks or discontinuities in function and first, second, and third order derivatives without artificial case related constants. However the new detector never mistakes high frequency waves, critical points and expansion waves as shock. This will overcome the bottle neck problem with numerical simulation for the shock-boundary layer interaction, shock-acoustic interaction, image process, porous media flow, multiple phase flow, detonation wave and anywhere the high frequency waves are important, but discontinuity exists and is mixed with high frequency waves. To introduce our new two step shock/discontinuity detector, we need to introduce some popular shock detectors first.

1) Harten's switch function and Jameson's shock detector

Harten (1978) defined an automatic switch function that is able to detect large changes in the variation of the function values f_i. It generates values between 0 and 1, where 0 is considered smooth and 1 is considered non-smooth.

The switch is defined as

$$\theta_{j+\frac{1}{2}} = \max\left(\hat{\theta}_j, \hat{\theta}_{j+1}\right), \tag{3.1}$$

with

$$\hat{\theta}_i = \begin{cases} \left| \dfrac{\left|\alpha_{i+\frac{1}{2}}\right| - \left|\alpha_{i-\frac{1}{2}}\right|}{\left|\alpha_{i+\frac{1}{2}}\right| + \left|\alpha_{i-\frac{1}{2}}\right|} \right|^p, & \text{if } \left|\alpha_{i+\frac{1}{2}}\right| + \left|\alpha_{i-\frac{1}{2}}\right| > \varepsilon, \\ 0, & \text{otherwise,} \end{cases}$$

where $\alpha_{i+1/2} = f_{i+1} - f_i$, and ε is a suitably chosen measure of insignificant variation in f.

Jameson's (1981) shock detector is similar, which can be described as:

$$\nu_i = \frac{|p_{i-1}-2p_i+p_{i+1}|}{|p_{i-1}|+2|p_i|+|p_{i+1}|}, \tag{3.2}$$

which is related to the second order derivative of the pressure.

2) WENO

The WENO weights use smoothness measurements that evaluate the changes in the variation of the function values f_i. Assuming that the three weights have equal contribution, we can determine that a function is smooth if all values are approximately $1/3$.

$$\omega_i = \alpha_i \Big(\sum_j \alpha_j\Big)^{-1}, \quad \alpha_i = (IS_i+\varepsilon)^{-2}, \quad i=0,1,2, \tag{3.3}$$

where

$$IS_0 = \frac{13}{12}(f_{i-2}-2f_{i-1}+f_i)^2+\frac{1}{4}(f_{i-2}-4f_{i-1}+3f_i)^2, \tag{3.4a}$$

$$IS_1 = \frac{13}{12}(f_{i-1}-2f_i+f_{i+1})^2+\frac{1}{4}(f_{i-1}-f_{i+1})^2, \tag{3.4b}$$

$$IS_2 = \frac{13}{12}(f_{i+2}-2f_{i+1}+f_i)^2+\frac{1}{4}(f_{i+2}-4f_{i+1}+3f_i)^2. \tag{3.4c}$$

3) New two step shock/discontinuity locator [13]

Step 1 Determine the multigrid ratio of the approximation of the sum of the 4^{th}, 5^{th} and 6^{th} truncation errors for [$F = f+$smooth sine wave of small amplitude] and select the points where the ratio is smaller than 4. Theoretically, the ratio of the 4^{th} order truncation error of coarse and fine grids should be 16, but any function that has a ratio of 4 will be considered smooth and passing the test. The points which have a ratio less than 4 will be picked out for the second left and right hand slope ratio check.

The multigrid truncation error ratio check is:

$$MR(i,h) = \frac{T_C(i,h)}{T_F(i,h)+\varepsilon},$$

where

$$T_C(i,h) = T_4(i,2h)+T_5(i,2h)+T_6(i,2h) = \frac{|f_i^{(4)}|(2h)^4}{4!}+\frac{|f_i^{(5)}|(2h)^5}{5!}+\frac{|f_i^{(6)}|(2h)^6}{6!}, \tag{3.5a}$$

$$T_F(i,h) = T_4(i,h)+T_5(i,h)+T_6(i,h) = \frac{|f_i^{(4)}|(h)^4}{4!}+\frac{|f_i^{(5)}|(h)^5}{5!}+\frac{|f_i^{(6)}|(h)^6}{6!}, \tag{3.5b}$$

where $T_F(i,h)$ is the truncation error sum (4^{th}, 5^{th} and 6^{th}) calculated at the fine grid with n points, $T_C(i,h)$ is the truncation error sum calculated at the coarse grid with $n/2$ points by Taylor expansion. $T_F(i,h)$ and $T_C(i,h)$ have 4^{th}, 5^{th} and 6^{th} order derivatives, which are all calculated by a 6^{th} order compact scheme.

Step 2 Calculate the local left and right slope ratio check only at the points which have first ratio less than 4.

The new local left and right slope ratio check is:

$$LR(i)=\left|\left|\frac{f'_R}{f'_L}\right|-\left|\frac{f'_L}{f'_R}\right|\right|\left(\left|\frac{f'_R}{f'_L}\right|+\left|\frac{f'_L}{f'_R}\right|+\varepsilon\right)^{-1}=\left|\frac{(f'_R)^2-(f'_L)^2}{(f'_R)^2+(f'_L)^2+\varepsilon}\right|=\left|\frac{\alpha_R^2-\alpha_L^2}{\alpha_R^2+\alpha_L^2+\varepsilon}\right|, \tag{3.6}$$

where $f'_R=3f_i-4f_{i+1}+f_{i+2}$, $f'_L=3f_i-4f_{i-1}+f_{i-2}$ and ε is a small number to avoid division by zero.

Step 3 Optional Step 3: Use a cutoff value of 0.8 to create a 0/1 switch function on the result of Step 2. If the value is zero, f is considered locally smooth, and if the value is one, f is a shock/discontinuity at that point.

Note that Liu's first step always checks $f+\sigma\sin(k\pi x+\phi)$ instead of f, where σ is a small number. Since all derivatives are calculated by a subroutine with a standard compact scheme, the cost of two step checks is relatively inexpensive.

In order to find a universal formula, we need to normalize the data set, $u(i)$, $i=1,\cdots,n$,

$$u_{diff}=|u_{\max}-u_{\min}|, \tag{3.7a}$$

$$\overline{u}=\frac{u-u_{\min}}{u_{diff}}. \tag{3.7b}$$

Here, $u_{\max}$ and $u_{\min}$ are the maximum and minimum values of u respectively and $\overline{u}$ is normalized. For simplicity, we disregard the hat of u and use $u(i)$ as the normalized data set. However, this normalization is for finding the shock locator only and not for the function itself which we calculate for derivatives.

3.2 Control function for using WENO to improve CS and UCS

3.2.1 Basic idea of the control function

The new shock detector can provide accurate location of shocks including weak shocks, strong shocks, oblique shocks and discontinuity in function, first, second and third order derivatives. However, the detector is a switch function and gives one in shock and zero for others. As we mentioned above, a switch function cannot be directly used to mix CS and WENO and we must develop a rather smooth function to mix CS (3.8a) and WENO (3.8b):

$$\frac{1}{3}H'_{j-\frac{3}{2}}+H'_{j-\frac{1}{2}}+\frac{1}{3}H'_{j+\frac{1}{2}}=\frac{1}{h}\Big[-\frac{1}{36}H'_{j-\frac{5}{2}}-\frac{7}{9}H'_{j-\frac{3}{2}}+\frac{7}{9}H'_{j+\frac{1}{2}}+\frac{1}{36}H'_{j+\frac{3}{2}}\Big], \tag{3.8a}$$

$$\begin{aligned}H'_{j-\frac{1}{2}}=&\omega_{0,j-\frac{1}{2}}\Big(\frac{1}{3}F_{j-3}-\frac{7}{6}F_{j-2}+\frac{11}{6}F_{j-1}\Big)+\omega_{1,j-\frac{1}{2}}\Big(-\frac{1}{6}F_{j-2}+\frac{5}{6}F_{j-1}+\frac{1}{3}F_j\Big)\\&+\omega_{2,j-\frac{1}{2}}\Big(\frac{1}{3}F_{j-1}+\frac{5}{6}F_j-\frac{1}{6}F_{j+1}\Big),\end{aligned} \tag{3.8b}$$

where F is the original function and H is a primitive function of F and H' is the flux $\hat{F}=H'$.

We defined a new control function Ω:

$$\Omega^* CS+(1-\Omega)^* WENO, \tag{3.9}$$

which will lead a tri-diagonal matrix system which is the core of our new scheme:

$$\begin{aligned}
&\frac{1}{3}\Omega H'_{j-\frac{3}{2}}+H'_{j-\frac{1}{2}}+\frac{1}{3}\Omega H'_{j+\frac{1}{2}}\\
=&\Omega*\Big[\frac{1}{36}\big(H'_{j+\frac{3}{2}}-H'_{j-\frac{5}{2}}\big)+\frac{7}{9}\big(H'_{j+\frac{1}{2}}-H'_{j-\frac{3}{2}}\big)\Big]+(1-\Omega)*\Big[\omega_{0,j-\frac{1}{2}}\Big(\frac{1}{3}F_{j-3}-\frac{7}{6}F_{j-2}+\frac{11}{6}F_{j-1}\Big)\\
&+\omega_{1,j-\frac{1}{2}}\Big(-\frac{1}{6}F_{j-2}+\frac{5}{6}F_{j-1}+\frac{1}{3}F_j\Big)+\omega_{2,j-\frac{1}{2}}\Big(\frac{1}{3}F_{j-1}+\frac{5}{6}F_j-\frac{1}{6}F_{j+1}\Big)\Big].
\end{aligned} \tag{3.10}$$

When $\Omega=1.0$, the equation becomes a standard sixth order compact scheme, but when $\Omega=0.0$ the scheme is a standard WENO scheme.

For the modified upwinding compact scheme (MUCS), the final matrix becomes:

$$\begin{aligned}
&\frac{1}{4}\Omega H'_{j-\frac{3}{2}}+H'_{j-\frac{1}{2}}+\frac{1}{2}\Omega H'_{j+\frac{1}{2}}\\
=&\Omega*\Big[-\frac{1}{60}H_{j-\frac{5}{2}}-\frac{31}{48}H_{j-\frac{3}{2}}-\frac{1}{3}H_{j-\frac{1}{2}}+\frac{11}{12}H_{j+\frac{1}{2}}+\frac{1}{12}H_{j+\frac{3}{2}}-\frac{1}{240}H_{j+\frac{5}{2}}\Big]\\
&+(1-\Omega)*\Big[\omega_{0,j-\frac{1}{2}}\Big(\frac{1}{3}F_{j-3}-\frac{7}{6}F_{j-2}+\frac{11}{6}F_{j-1}\Big)+\omega_{1,j-\frac{1}{2}}\Big(-\frac{1}{6}F_{j-2}+\frac{5}{6}F_{j-1}+\frac{1}{3}F_j\Big)\\
&+\omega_{2,j-\frac{1}{2}}\Big(\frac{1}{3}F_{j-1}+\frac{5}{6}F_j-\frac{1}{6}F_{j+1}\Big)\Big].
\end{aligned} \tag{3.11}$$

3.2.2 Construction of the control function

In our new shock detector, we define

$$MR(i,h)=\frac{T_C(i,h)}{T_F(i,h)+\varepsilon}$$

as a ratio of coarse grid truncation over find grid truncation. MR should be around 16.0 if the function has at least 6^{th} order continuous derivatives. Here we define

$$\Omega=1.0-\min\Big\{1.0,\frac{8.0}{MR(i,h)}\Big\}*LR, \tag{3.12}$$

where MR is the multigrid global truncation error ratio and LR is the local ratio of left and right side angle ratio. If the shock is met, MR is small, LR is 1 and Ω=0.0, The WENO will be used and the CS is fully blocked. If the area is smooth, MR should be around 16.0 and LR is close to zero (left and right angle are same). Additional requirements are set such that any point must compare with left and right neighboring points. We pick the largest Ω among the three neighboring points.

The reason we pick $MR=8.0$ is that we treat the fourth order continuous function as smooth function and only need half of LR for Ω. It is easy to find that there are no case related adjustable coefficients which is quite different from many other published hybrid schemes. The shock detector is very reliable and the new scheme is very robust which can be found from the examples of our computation.

4 Computational results by MUCS

4.1 MUCS for 2-D Euler equations

An incident shock case with an inflow Mach number of 2 and attach angle of $\vartheta=35.241^\circ$ was chosen as a sample problem to compare the WENO and MUCS results with the exact solution. Since the incident shock has exact solution, it is a good prototype problem for scheme validation. It is also a difficult problem to get sharp shocks without visible oscillation for any high order scheme. Three sizes of grids are selected, 33×33 as coarse, 65×65 as middle, and 129×129 as fine. The computational domain is $x=2.0$ and $y=1.1$ and a uniform grids was used. We find that a modified compact scheme (MCS) worked well on coarse and middle size grids, but has oscillations on the fine grids (129×129). However, modified upwinding compact scheme or MUCS does not have serious oscillation, even better than WENO after the second shock. On the other hand MUCS captured the shock sharper than WENO for all grids. The control (mixing) function did use WENO (red area) to block the UCS and used UCS for smooth area (blue area). All of the comparisons are made by using same code and same boundary treatment but different subroutines (WENO or MUCS) for derivatives only. Figs. 2 and 3 provide the numerical results and comparison on a coarse grid of 33×33. Figs. 4 and 5 give the numerical results and comparison on a middle grid of 65×65. The fine grid of 129×129 results are depicted on Figs. 6-8. From these figures we can find the 7^{th} order MUCS results are very comparable with the exact solution and are better than that obtained by 5^{th} order WENO scheme.

4.2 MUCS for 2-D shock boundary layer interaction

4.2.1 2-D N-S code validation

In order to test if the current code can work for 2-D and 3-D shock-boundary layer interaction, a 2-D incident shock-boundary layer interaction (Fig. 9) was studied by the current code (Xie et al. 2009). The Reynolds number is 10^5 and the Mach number was set to 2.15. The overall pressure ratio is 1.55. For comparison, the inflow condition was set as that investigated by Degrez et al. (1987). Their experimental work has shown that the shock-boundary layer interaction is laminar and two-dimensional. Therefore, we can do a 2-D numerical simulation and compare with their computational and experimental results. The computational grids is 257×257. The grid stretching in the streamwise direction is 1.01. The stretching in normal direction is 1.015. A 2-D Navier-Stokes equation is solved as the governing equation. Fig. 10 shows the computational results by current

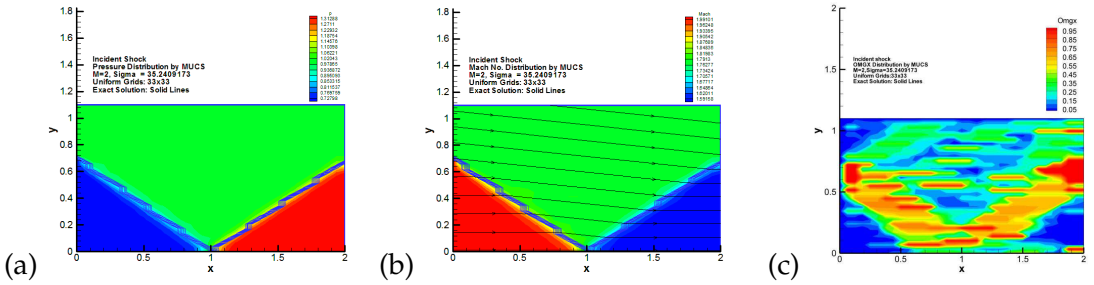

Figure 2: Numerical test for 2-D incident shock on an 33×33 grid. (a) Pressure contour; (b) Mach number; (c) control function (red is WENO and blue is UCS).

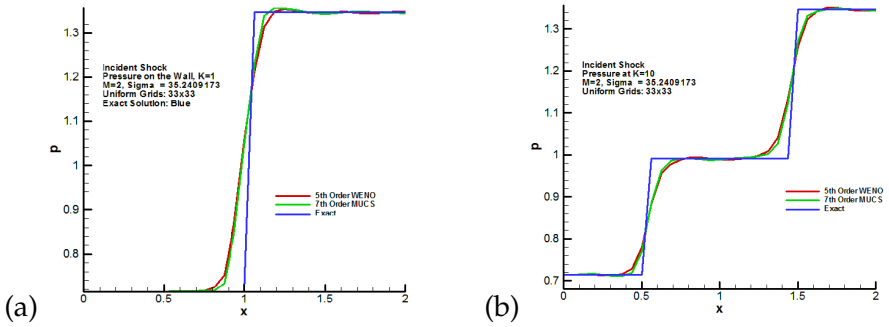

Figure 3: Pressure distribution on coarse grids (33×33). (a) On the wall $k=1$; (b) $k=10$.

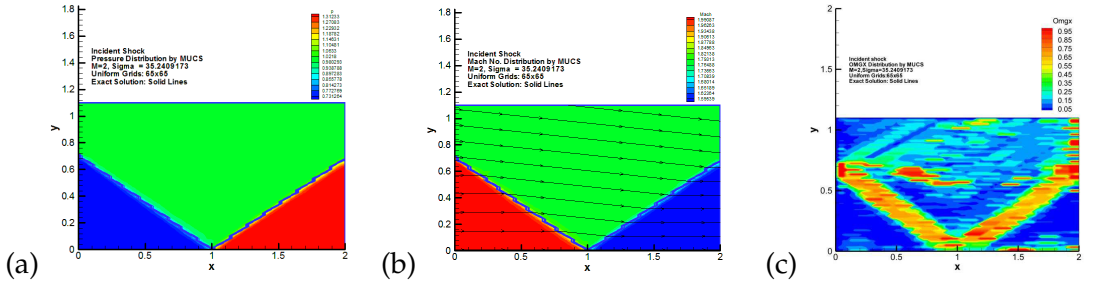

Figure 4: Same as Fig. 2 except on an 65×65 grid.

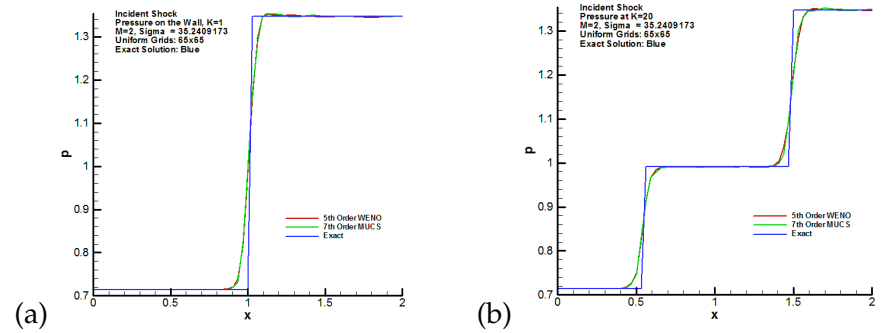

Figure 5: Pressure distribution on middle grids (65×65). (a) On the wall $k=1$; (b) $k=20$.

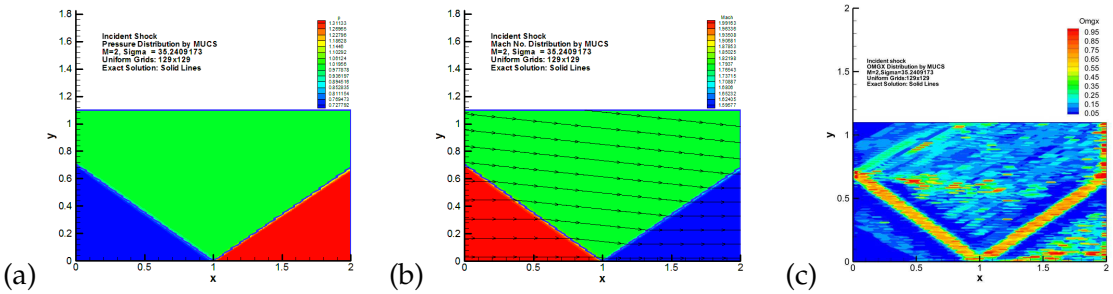

Figure 6: Same as Fig. 2 except on an 129×129 grid.

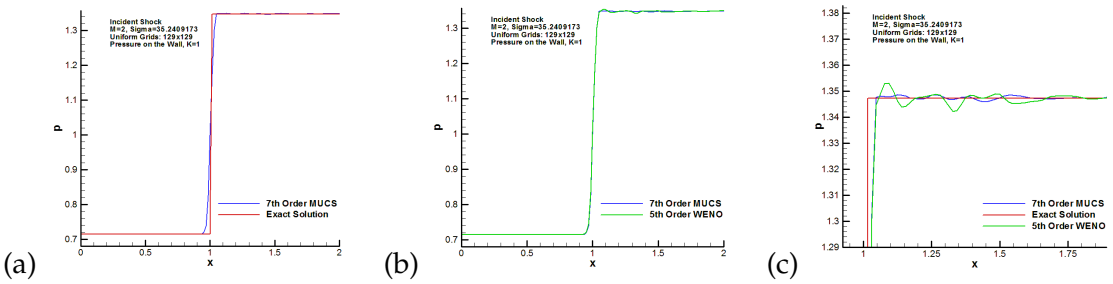

Figure 7: Pressure distribution at wall $(k=1)$ on fine grids (129×129). (a) 7^{th} order MUCS and exact; (b) 7^{th} order MUCS and 5^{th} order WENO; (c) locally enlarged comparison.

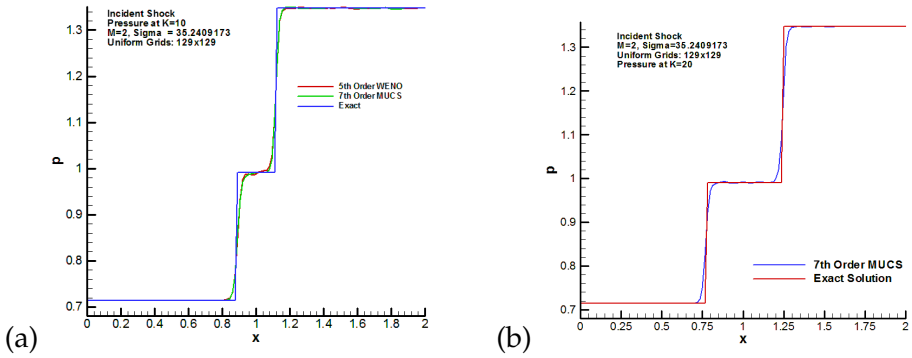

Figure 8: Pressure distribution on fine grids (129×129). (a) $k=10$; (b) $k=20$.

code and Fig. 11 gives a comparison of our computational results with the results given by Degrez et al. It is observed that Degrez's computation did not match his experimental results well, and our computational results do not match very well either. However, the discrepancy between computation and experiment is in the acceptable range.

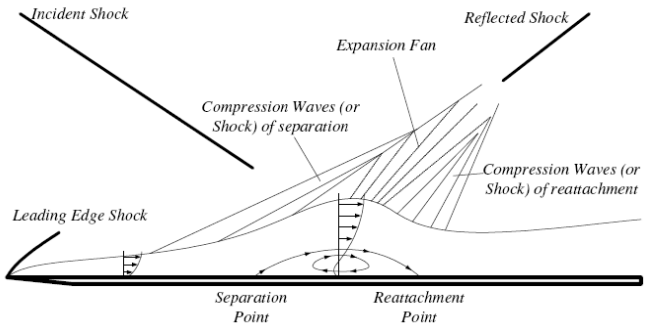

Figure 9: Sketch of incident shock-boundary layer interaction.

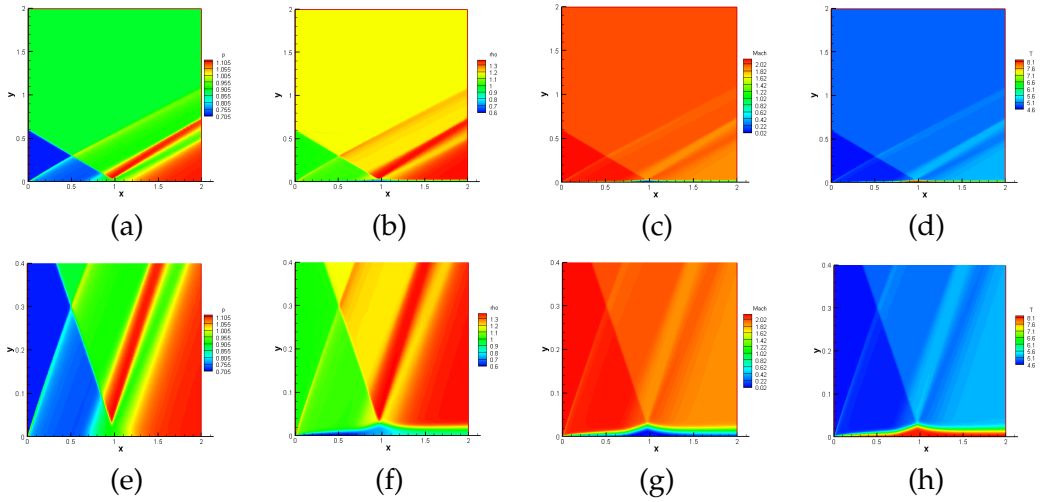

Figure 10: Top is a normal view. (a) Pressure distribution; (b) density distribution; (c) Mach number distribution; (d) temperature distribution. Bottom is stretched in the normal direction by a factor of 5. (e) Pressure distribution; (f) density distribution; (g) Mach number distribution; (h) temperature distribution.

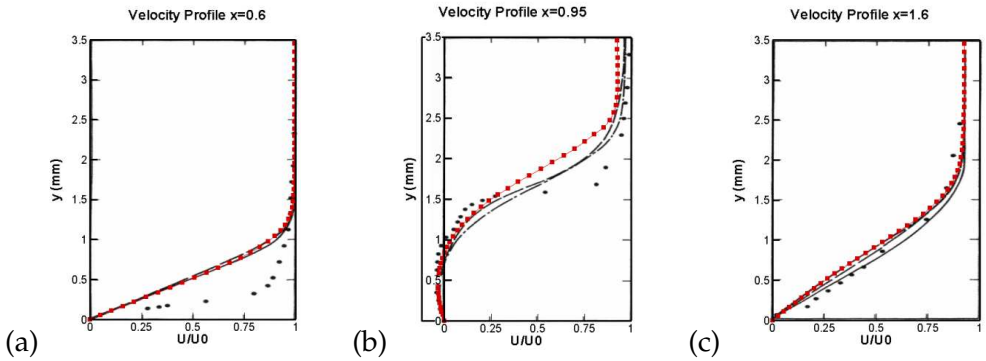

Figure 11: Comparison of velocity profiles at different locations. (The red one is our computation, the black solid line and black square are Degrez's computation and experiment respectively.)

4.2.2 Computation of 2-D incident shock-boundary layer interaction

In order to compare the performance of our MUCS scheme with standard WENO, we select an incident shock case with Mach number 3 and Reynolds number $Re=3\times10^4$ and the attack angle $\vartheta=32.24^\circ$. Three grids were selected: 33×33 as coarse, 65×65 as middle, and 129×129 as fine. The solution at a grid of 257×257 is considered as a reference solution. Fig. 12 gives a distribution contour for pressure with stream track. The incident shock, leading shock, separation shock, expansion waves and reflecting shock are all clearly captured. A structure of separation bubble with 5 vertexes is captured. Fig. 13 depicts the distribution of control function of OMGX and OMGZ in x- and z- directions. The blue area is the area where compact scheme was used and the red area represents the area where the WENO scheme was applied. Here, we use the results of grids 257×257 as a reference. Figs. 14 and 15 provide a distribution of pressure, control functions OMGX, OMGZ, obtained by MUCS on a grid of 129×129. The results on the grids of 129×129 by MUCS agree well with our reference results. Fig. 16 gives a comparison of 7^{th} order MUCS and 5^{th} order WENO schemes with the reference results on the pressure distribution on the surface wall. It can be found that the results obtained by MUCS are closer to the reference results. Table 1 provides a comparison of the size of the separation bubbles on three grid levels and it is found that the grid convergence is acceptable. All comparisons are made by a same code at same time step with different schemes and different grids.

Table 1: Size of separation bubbles caused by shock/boundary layer interaction.

Grid Number	65×65	129×129	257×257
Size of separation bubbles	1.10	1.01	0.97

4.3 Problems with compact scheme and modified compact scheme (MCS)

For the 2-D Euler solver, the pressure distribution contour obtained by MCS looks fine. However, MCS has a serious problem with artificial oscillations around the shock. Since the MCS will become a compact scheme in the smooth area which is non-dissipative, any low frequency error wave generated by shock overshooting will never be damped (Fig. 18). Since the wave generated by numerical shock overshooting, which is in the range of grid resolution, the error wave will remain forever if MCS is used. However, if we use MUCS, the scheme becomes UCS which has dissipation after the shock and the numerical shock overshooting will be damped quickly and the physical solution can be obtained.

There is a serious question if the high order central compact scheme along with the high order filter can still be used for DNS or LES for shock boundary layer interaction? Unfortunately, we have to conclude that, in general, the numerical method of the high order compact scheme along with the high order filter may not be useable for high order DNS or LES for shocks.

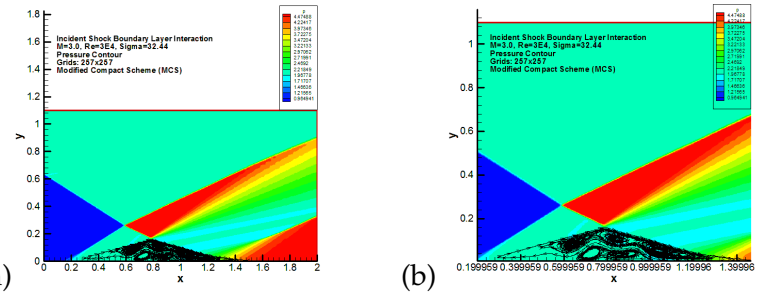

Figure 12: (a) Pressure distribution and stream traces by MUCS on grid of 257×257 as reference; (b) locally enlarged.

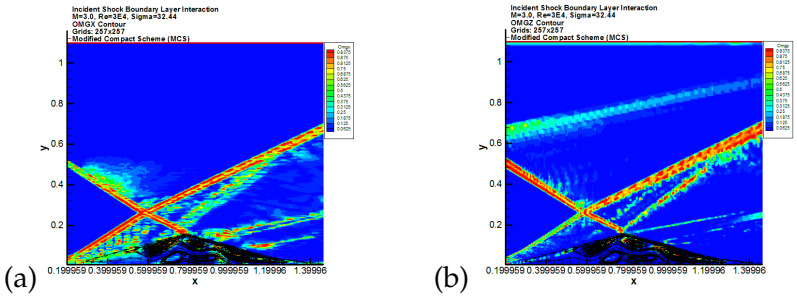

Figure 13: Control function on girds of 257×257. (a) Omega in x-direction; (b) Omega in z-direction (red area is WENO and blue area is UCS).

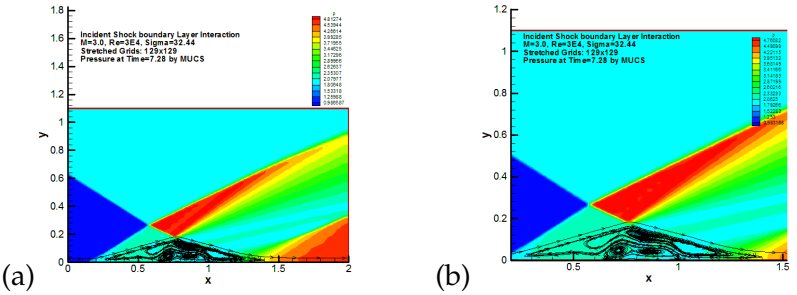

Figure 14: Pressure distribution obtained by MUCS on grids of 129×129. (a) Regular; (b) locally enlarged.

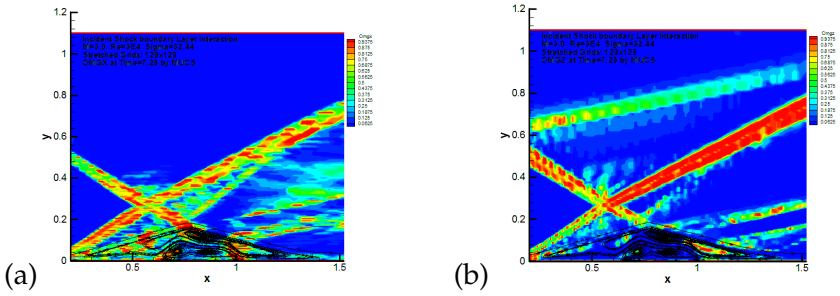

Figure 15: Control function on girds of 129×129. (a) Omega in x-direction; (b) Omega in z-direction (red area is WENO and blue area is UCS).

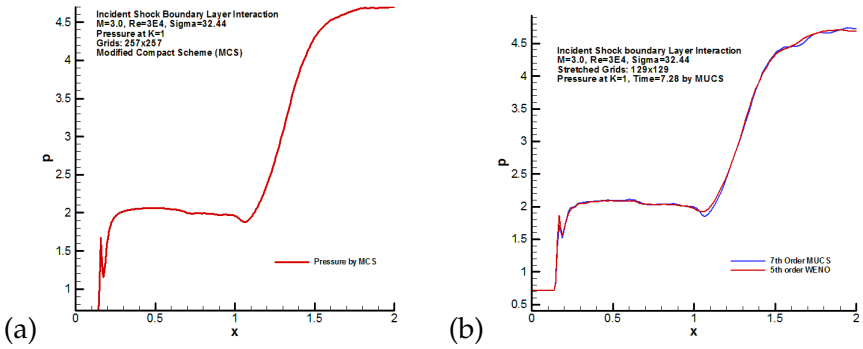

Figure 16: Pressure distribution on the wall. (a) Results on grids of 257×257 as reference; (b) comparison of 7^{th} order MUCS and 5^{th} order WENO on grid 129×129.

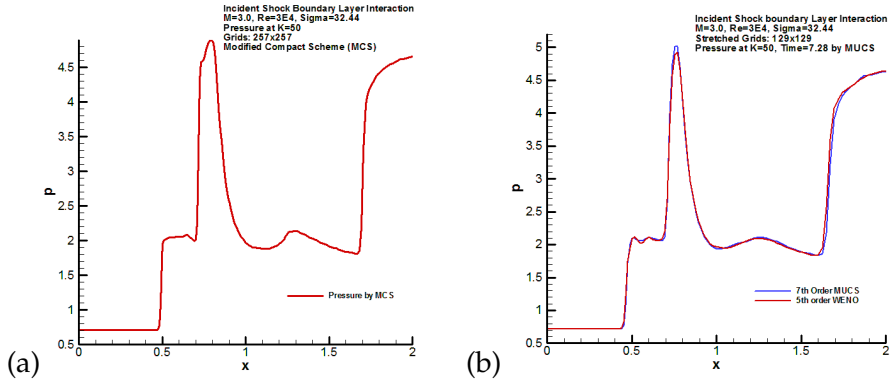

Figure 17: Pressure distribution. (a) Results on grids of 257×257 at $k=50$ as reference; (b) comparison of 7^{th} order MUCS and 5^{th} order WENO on grid 129×129 at $k=50$.

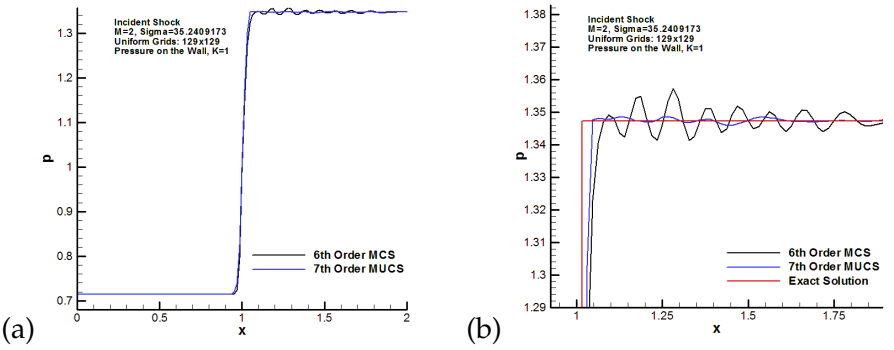

Figure 18: Problems with modified compact scheme (MCS) for 2-D Euler equation on grids of 129×129. (a) Comparison of MCS and MUCS; (b) locally enlarged comparison of MCS, MUCS, and exact solution.

5 Conclusions

Modified up-winding compact scheme (MUCS) with a new shock detector and new mixing function, which uses WENO to improve upwind compact scheme, can be used for

Euler and Navier-Stokes equations for sharp shock capturing and high resolution for small length scales. The new scheme, MUCS, does not have case-related parameters. Modified central compact scheme (MCS) may give better resolution for shock-boundary layer interaction than MUCS, but it failed to pass the test for the fine grid Euler equation. The problem with MCS is that the central compact scheme does not have dissipation and cannot damp the numerical oscillations caused by the shock overshooting. On the other hand, the high order filter can only remove high frequency numerical errors. Once the low frequency error is generated by the numerical scheme, CS cannot remove them. Therefore, unfortunately, high order CS along with high order filter cannot work well for DNS or LES for high speed flow with a shock. Modified central compact scheme (MCS) needs further improvement to pass the fine grid check for the Euler equations. Additional carefully selected dissipations may be needed for MCS.

Acknowledgments

This work is supported by AFRL VA Summer Faculty Research Program. The authors thank Drs. Poggie, Gaitonde, Visbal for their support through VA Summer Faculty Program.

References

[1] B. Costaa and W. S. Don, High order hybrid central-WENO finite difference scheme for conservation laws, J. Comput. Appl. Math., 204 (2007), 209–218.
[2] D. Gaitonde and M. Visbal, Pade-type high-order boundary filters for the Navier-Stokes equations, AIAA J., 38(11) (2000), 2103–2112.
[3] D. Gaitonde, P. W. Canupp and M. Holden, Heat transfer predictions in a laminar hypersonic viscous/inviscid interaction, J. Thermophys. Heat Trans., 16(4) (2002), 481–489.
[4] S. K. Godunov, A difference scheme for numerical computation of discontinuous solution of hydrodynamic equations, Math. Sbornik., 47 (1969), 271–306, (in Russian) translated US Joint Publ. Res. Service, JPRS 7226, 1969.
[5] A. Harten, High resolution schemes for hyperbolic conservation laws, J. Comput. Phys., 49 (1983), 357–393.
[6] A. Harten, B. Engquist, B. Osher and Sr. Charkravarthy, Uniformly high order accurate essentially non-oscillatory schemes III, J. Comput. Phys., 71 (1987), 231–303.
[7] G. S. Jiang and C. W. Shu, Efficient implementation of weighted ENO scheme, J. Comput. Phys., 126 (1996), 202–228.
[8] L. Jiang, H. Shan and C. Liu, Weight compact scheme for shock capturing, Int. J. Comput. Fluid Dyn., 15 (2001), 147–155.
[9] D. Kim and J. Kwon, A high-order accurate hybrid scheme using a central flux scheme and a WENO scheme for compressible flowfield analysis, J. Comput. Phys., 210 (2005), 554–583.
[10] S. K. Lele, Compact finite difference schemes with spectral-like resolution, J. Comput. Phys., 103 (1992), 16–42.
[11] C. Liu, P. Xie and M. Olveira, High order modified compact scheme for high speed flow, Technical Report to Gaitonde at Air Force Research Lab.

[12] X.-D. Liu, S. Osher and T. Chan, Weighted essentially nonoscilltory schemes, J. Comput. Phys., 115 (1994), 200–212.
[13] M. Oliveira1, P. Lu, X. Liu and C. Liu, A new shock/discontinuity detector, Int. J. Comput. Math., 87 (2010), 3063–3078.
[14] Y. Ren, M. Liu and H. Zhang, A characteristic-wise hybrid compact-WENO scheme for solving hyperbolic conservation laws, J. Comput. Phys., 192 (2003), 365–386.
[15] P. L. Roe, Approximate Riemann solvers, parameter vectors and difference schemes, J. Comput. Phys., 43 (1981), 357–372.
[16] Y. V. S. S. Sanyasiraju and N. Mishra, Exponential compact higher order scheme for nonlinear steady convection-diffusion equations, Commun. Comput. Phys., 9 (2011), 897–916.
[17] C. W. Shu and S. Osher, Efficient implementation of essentially non-oscillatory shock-capturing scheme, J. Comput. Phys., 77 (1988), 439–471.
[18] C. W. Shu and S. Osher, Efficient implementation of essentially non-oscillatory shock-capturing schemes II, J. Comput. Phys., 83 (1989), 32–78.
[19] J. Su, M. Oliveira, P. Xie and C. Liu, Error analysis for weighted higher order compact finite difference scheme, J. Appl. Math. Sci., 1 (2007), 2863–2881.
[20] S. Tu, G. W. Skelton and Q. Pang, A compact high order space-time method for conservation laws, Commun. Comput. Phys., 9 (2011), 441–480.
[21] B. Van Leer, Towards the ultimate conservative difference scheme V: a second order sequel to Godunov's scheme, J. Comput. Phys., 32 (1979), 101–136.
[22] M. Visbal and D. Gaitonde, On the use of higher-order finite-difference schemes on curvilinear and deforming mashes, J. Comput. Phys., 181 (2002), 155–158.
[23] T. P. Wadhams and M. S. Holden, Summary of experimental studies for code validation in the LENS facility with recent Navier-Stokes and DSMC solutions for two- and three- dimensional separated regions in hypervelocity flows, AIAA 2004-917 42nd AIAA Aerospace Sciences Meeting and Exhibit, 5-8 January 2004, Reno, Nevada.
[24] P. Xie, M. Oliveira, J. Su and C. Liu, High order weighted compact schemes for shock/boundary layer interaction, AIAA-2008-0754, January 2008.